

Electronic Supplementary Information for

Laser flash photolysis study of the photoinduced oxidation of 4-(dimethylamino)benzonitrile (DMABN)

*Frank Leresche,^{†, ‡, §} Lucie Ludviková,[‡] Dominik Heger,[‡] Petr Klán,[‡] Urs von Gunten ^{†, ‡} and
Silvio Canonica[†],*

[†]Eawag, Swiss Federal Institute of Aquatic Science and Technology, Ueberlandstrasse 133,
CH-8600 Dübendorf, Switzerland

[‡]School of Architecture, Civil and Environmental Engineering (ENAC), Ecole Polytechnique
Fédérale de Lausanne (EPFL), CH-1015 Lausanne, Switzerland

[‡]Department of Chemistry and RECETOX, Faculty of Science, Masaryk University,
Kamenice 5, 62500 Brno, Czech Republic

[§]Present address: Department of Civil, Environmental and Architectural Engineering, University
of Colorado, Boulder, CO 80309, USA

Number of pages:	27
Number of text sections:	10
Number of figures:	12
Number of tables:	8

* Corresponding Authors:

SC: Telephone: +41-58-765-5453. E-mail: silvio.canonica@eawag.ch.

DH: Tel: +420 54949 3322. E-mail: hegerd@chemi.muni.cz

Text S1. List of chemicals

4-(Dimethylamino)benzotrile (DMABN, Aldrich, 98%), NaH₂PO₄·2H₂O (Lachner, 100%), Na₂HPO₄·12H₂O (Lachner, 99.3%), H₃PO₄ (Lachema, 85%), NaNO₂ (Lachema, 98%), acetonitrile (Sigma Aldrich, HPLC grade), triethanolamine (TEA, Sigma, 99%), O₂ (Siad, technical 2.5), N₂O (Siad, 99.99%).

Photosensitizers: 9,10-Anthraquinone-1,5-disulfonate (AQdS, ABCR 98%), 2-acetonaphthone (2-AN, Sigma-Aldrich, 99%), 1-acetonaphthone (1-AN, Sigma-Aldrich, 97%), 1-naphthaldehyde (1-NA, Aldrich, 95%), thionine acetate salt (THI, Sigma, for microscopy), 3-methoxyacetophenone (3-MA, Fluka 97%).

Table S1. Observation wavelengths used in LFP kinetic measurements to determine the decay rate constants of transient species

Transient Species	Observation wavelength /nm
<i>Excitation Wavelength 266nm</i>	
³ DMABN*	400 or 600
DMABN ⁺⁺	500
Hydrated electron (<i>e</i> _{aq} ⁻)	600 or 700
<i>Excitation Wavelength 355 or 532 nm</i>	
DMABN ⁺⁺	500 or 520
9,10-Anthraquinone-1,5-disulfonate triplet (³ AQdS*)	420 or 470
9,10-Anthraquinone-1,5-disulfonate radical anion (AQdS ^{•-})	500
2-Acetonaphthone triplet (³ 2-AN*)	440
2-Acetonaphthone radical anion (2-AN ^{•-})	400
1-Naphthaldehyde triplet (³ 1-NA*)	600
1-Naphthaldehyde radical anion (1-NA ^{•-})	400
3-Methoxyacetophenone triplet (³ 3-MOAP*)	400
Thionine triplet (³ THI*)	670
Thionine radical anion (THI ^{•-})	400
1-Acetonaphthone triplet (³ 1-AN*)	500

Text S2. Kinetic modelling of the decay of the hydrated electron and the radical cation of DMABN (DMABN^{•+}) after direct photoionization

Model compilation

The kinetic modelling was performed using the software Kintecus¹. The following concentrations were used:

$$[\text{DMABN}] = 1.33 \times 10^{-4} \text{ M};$$

$$\text{Initial concentrations of DMABN}^{\bullet+} \text{ and } e_{\text{aq}}^- \text{ (hydrated electron)} = 2 \times 10^{-6} \text{ M};$$

$$\text{For O}_2\text{-purged solution: } [\text{O}_2] = 1.23 \times 10^{-3} \text{ M};$$

$$\text{For aerated solution: } [\text{O}_2] = 2.58 \times 10^{-4} \text{ M};$$

$$\text{For N}_2\text{O-purged solution: } [\text{N}_2\text{O}] = 2.7 \times 10^{-2} \text{ M}.$$

The concentration of $[\text{H}_2\text{PO}_4^-]$ and $[\text{HPO}_4^{2-}]$ was adjusted to the given pH using the pK_a value of 7.21 and $[\text{H}_2\text{PO}_4^-] + [\text{HPO}_4^{2-}] = 2 \times 10^{-3} \text{ M}$. The rate constants for acid–base speciation were calculated from the corresponding pK_a using a rate constant for the protonation reaction of $5 \times 10^9 \text{ M}^{-1} \text{ s}^{-1}$.

The concentration of $[\text{H}^+]$ and $[\text{OH}^-]$ were calculated from the pH and fixed as constants during the calculations.

Model explanations

The initial concentrations of $\text{DMABN}^{\bullet+}$ and e_{aq}^- , assumed to be equal, were chosen to approximately match the values obtained from the "initial" (i.e., within $\approx 10 \text{ ns}$ after the laser pulse) e_{aq}^- absorption in the laser flash photolysis experiments. In aerated or O_2 -purged solution, the main decay pathway for e_{aq}^- is its reaction with oxygen to form the superoxide radical anion ($\text{O}_2^{\bullet-}$, equation A1). The relative importance of a particular reaction was assessed by inserting dummy reaction products in the equations (e.g. for Equation A1, one could insert such a dummy reaction product X by writing the equation as: $e_{\text{aq}}^- + \text{O}_2 \rightleftharpoons \text{O}_2^{\bullet-} + \text{X}$), and monitoring the formation of this dummy product (which was not subject to any other reaction).

In experiments with degassed solutions the main decay pathway for the hydrated electron is most probably its reaction with DMABN to form a radical anion of DMABN (Equation A9).² However, such a radical anion could not be observed. The reactivity of the hydrated electron with water or with constituents of the buffer was of minor importance in our system (Equations A4–A8; A10–A12).

The fate of the radical cation of DMABN ($\text{DMABN}^{\bullet+}$) was assumed to be determined either by reduction reactions with the superoxide radical anion (Equation A13) or the hydrated electron (Equation A2) to give back the parent compound DMABN, or by formally unimolecular transformation (Equation A14) to form a hypothetical intermediate ($\text{DMABN}_{\text{trans}}$) and eventually the demethylated product of DMABN, 4-(methylamino)benzonitrile (MABN), which was observed in a previous steady-state irradiation study.³ In the model we did not include further reactions describing the mechanism of formation of MABN because of the missing constants of these still hypothetical reactions, described in detail in Ref. 3.

Table S2. Reaction equations and rate constants used for the modelling of the direct photoionization of DMABN

No	Reaction	Rate constant	Comment	Ref.
Hydrated electron (e_{aq}^-) reactions				
A1	$e_{aq}^- + O_2 \rightleftharpoons O_2^{\bullet -}$	$2 \times 10^{10} \text{ M}^{-1} \text{ s}^{-1}$		4
A2	$e_{aq}^- + \text{DMABN}^{\bullet +} \rightleftharpoons \text{DMABN}$	$1 \times 10^{10} \text{ M}^{-1} \text{ s}^{-1}$	Estimation	
A3	$e_{aq}^- + N_2O \rightleftharpoons OH^{\bullet} + N_2 + OH^-$	$9.1 \times 10^9 \text{ M}^{-1} \text{ s}^{-1}$		5
A4	$e_{aq}^- + e_{aq}^- \rightleftharpoons H_2 + 2 OH^-$	$5.5 \times 10^9 \text{ M}^{-1} \text{ s}^{-1}$		6
A5	$e_{aq}^- + Na^+ \rightleftharpoons Na$	$2 \times 10^4 \text{ M}^{-1} \text{ s}^{-1}$		6
A6	$e_{aq}^- + H^+ \rightleftharpoons H^{\bullet}$	$2.3 \times 10^{10} \text{ M}^{-1} \text{ s}^{-1}$		6
A7	$e_{aq}^- + H^{\bullet} \rightleftharpoons H_2 + OH^-$	$2.5 \times 10^{10} \text{ M}^{-1} \text{ s}^{-1}$		6
A8	$e_{aq}^- + OH^{\bullet} \rightleftharpoons OH^-$	$3 \times 10^{10} \text{ M}^{-1} \text{ s}^{-1}$		6
A9	$e_{aq}^- + \text{DMABN} \rightleftharpoons \text{DMABN}^{\bullet -}$	$1.4 \times 10^{10} \text{ M}^{-1} \text{ s}^{-1}$	Value for 4-methyl-benzonitrile	6
A10	$e_{aq}^- + H_2O \rightleftharpoons H^{\bullet} + OH^-$	$20 \text{ M}^{-1} \text{ s}^{-1}$		6
A11	$e_{aq}^- + H_2PO_4^- \rightleftharpoons H^{\bullet} + HPO_4^{2-}$	$1.9 \times 10^7 \text{ M}^{-1} \text{ s}^{-1}$		6
A12	$e_{aq}^- + HPO_4^{2-} \rightleftharpoons H^{\bullet} + PO_4^{3-}$	$1.4 \times 10^5 \text{ M}^{-1} \text{ s}^{-1}$		6
DMABN$^{\bullet +}$ reactions				
A13	$\text{DMABN}^{\bullet +} + O_2^{\bullet -} \rightleftharpoons \text{DMABN} + O_2$	$1 \times 10^{10} \text{ M}^{-1} \text{ s}^{-1}$	From DMABN $^{\bullet +}$ decay in aerated solution	this study
A14	$\text{DMABN}^{\bullet +} \rightleftharpoons \text{DMABN}_{\text{trans}}$	$5 \times 10^3 \text{ s}^{-1}$	From DMABN $^{\bullet +}$ decay in degassed solution	this study
A15	$\text{DMABN}^{\bullet +} + \text{DMABN}^{\bullet -} \rightleftharpoons 2 \text{DMABN}$	$5 \times 10^9 \text{ M}^{-1} \text{ s}^{-1}$	Estimation	
Other reactions				
A16	$H^{\bullet} + OH^{\bullet} \rightleftharpoons H_2O$	$7 \times 10^9 \text{ M}^{-1} \text{ s}^{-1}$		6
A17	$O_2^{\bullet -} + H^+ \rightleftharpoons HO_2^{\bullet}$	$5 \times 10^9 \text{ M}^{-1} \text{ s}^{-1}$	From $pK_a = 4.8$	4
A18	$HO_2^{\bullet} \rightleftharpoons O_2^{\bullet -} + H^+$	$7.5 \times 10^4 \text{ s}^{-1}$		4
A19	$HO_2^{\bullet} + HO_2^{\bullet} \rightleftharpoons H_2O_2 + O_2$	$8.3 \times 10^5 \text{ M}^{-1} \text{ s}^{-1}$		4
A20	$HO_2^{\bullet} + O_2^{\bullet -} \rightleftharpoons HO_2^- + O_2$	$9.7 \times 10^7 \text{ M}^{-1} \text{ s}^{-1}$		4
A21	$H_2O_2 \rightleftharpoons HO_2^- + H^+$	$1.2 \times 10^{-2} \text{ s}^{-1}$	From $pK_a = 11.62$	7
A22	$HO_2^- + H^+ \rightleftharpoons H_2O_2$	$5 \times 10^9 \text{ M}^{-1} \text{ s}^{-1}$		7
A23	$\text{DMABN} + OH^{\bullet} \rightleftharpoons \text{DMABNOH}$	$5 \times 10^9 \text{ M}^{-1} \text{ s}^{-1}$	Estimation	
A24	$\text{DMABN}^{\bullet -} + O_2 \rightleftharpoons \text{DMABN} + O_2^{\bullet -}$	$3 \times 10^9 \text{ M}^{-1} \text{ s}^{-1}$	Estimation	

Text S3. Kinetic modelling of the decay of the radical cation of DMABN (DMABN^{•+}) formed through photosensitization by 1-naphthaldehyde (1-NA)

Model compilation

The modelling was performed using the software Kintecus¹. The following conditions were used:

$[\text{DMABN}] = 5.0 \times 10^{-4} \text{ M}$; $[\text{O}_2] = 2.80 \times 10^{-4} \text{ M}$; $[\text{H}^+] = 1.0 \times 10^{-8} \text{ M}$; $[\text{OH}^-] = 1.0 \times 10^{-6} \text{ M}$.

The rate constant for deprotonation reactions were calculated from the acid-base equilibrium constants using a rate constant for the protonation reaction of $5 \times 10^9 \text{ M}^{-1} \text{ s}^{-1}$.

The modeled decay rate constants were retrieved from the Kintecus model results by fitting $\ln(c/c_{\text{start}})$ vs time. The fittings were performed excluding the initial part of the decay to avoid incorporating fast second-order kinetic components, and using $c_{\text{start}} = 0.5 \times c_0$, where c_0 is the concentration of a given species at the beginning of the kinetic model calculation.

Model explanations

The decay of the triplet state of 1-NA ($^3\text{1-NA}^*$) is dominated by its reaction with DMABN (Equation B1), with a non-negligible (21%) contribution of quenching by O_2 (Equation B2).

As the fraction of $^3\text{1-NA}^*$ undergoing quenching by DMABN through energy loss (Equation 19 in the main paper) is not known, Equation B1 was written by neglecting this deactivation channel of $^3\text{1-NA}^*$ and assuming that the rate constants for quenching of $^3\text{1-NA}^*$ by DMABN and for reactive quenching leading to DMABN^{•+} formation are identical.

Similarly, the model does not take into account other deactivation pathways for $^3\text{1-NA}^*$ such as triplet–triplet annihilation and the various unimolecular deactivation channels, but these should be negligible under the present experimental conditions.

Regarding the quenching of $^3\text{1-NA}^*$ by O_2 , no distinction between the energy transfer pathway yielding $^1\text{O}_2$ and the energy loss pathway was done, because $^1\text{O}_2$ is not expected to react with any of the relevant species in solution. Moreover, a possible reactive quenching (leading to the transformation of 1-NA) was neglected.

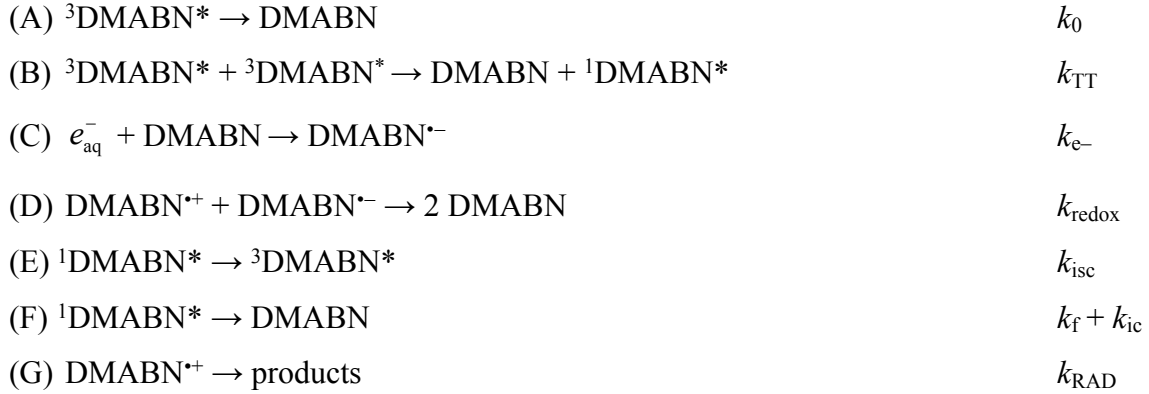
The decay of DMABN^{•+} is assumed to be determined by the reactions with the radical anion of 1-NA ($\text{1-NA}^{\bullet-}$) and $\text{O}_2^{\bullet-}$ (Equations B5 and B6) and by formally unimolecular transformation (Equation B7), similarly as described above (Text S2).

Table S3. Reaction equations and rate constants used for modelling the decay of the radical cation of DMABN (DMABN^{•+}) formed by 1-naphthaldehyde photosensitization

No	Reaction	Rate constant	Comment	Ref.
Triplet state of 1-naphthaldehyde decay and singlet oxygen				
B1	$^3\text{1-NA}^* + \text{DMABN} \rightleftharpoons \text{DMABN}^{\bullet+} + \text{1-NA}^{\bullet-}$	$3.4 \times 10^9 \text{ M}^{-1} \text{ s}^{-1}$	This paper	
B2	$^3\text{1-NA}^* + \text{O}_2 \rightleftharpoons \text{1-NA} + \text{products}$	$1.8 \times 10^9 \text{ M}^{-1} \text{ s}^{-1}$	Estimation from $^3\text{1-NA}^*$ lifetime	
B3	(not used)			
B4	$\text{1-NA}^{\bullet-} + \text{O}_2 \rightleftharpoons \text{1-NA} + \text{O}_2^{\bullet-}$	$3.4 \times 10^9 \text{ M}^{-1} \text{ s}^{-1}$	Estimation	
Reactions of DMABN^{•+}				
B5	$\text{DMABN}^{\bullet+} + \text{1-NA}^{\bullet-} \rightleftharpoons \text{DMABN} + \text{1-NA}$	$4 \times 10^9 \text{ M}^{-1} \text{ s}^{-1}$	Estimation	
B6	$\text{DMABN}^{\bullet+} + \text{O}_2^{\bullet-} \rightleftharpoons \text{DMABN} + \text{O}_2$	$1 \times 10^{10} \text{ M}^{-1} \text{ s}^{-1}$	Estimation	
B7	$\text{DMABN}^{\bullet+} \rightleftharpoons \text{DMABN}_{\text{trans}}$	$5 \times 10^3 \text{ s}^{-1}$	From DMABN ^{•+} decay in degassed solution after direct photoexcitation (266 nm)	
Other reactions				
B8	$\text{O}_2^{\bullet-} + \text{H}^+ \rightleftharpoons \text{HO}_2^{\bullet}$	$5 \times 10^9 \text{ M}^{-1} \text{ s}^{-1}$	From pK _a 4.8	4
B9	$\text{HO}_2^{\bullet} \rightleftharpoons \text{O}_2^{\bullet-} + \text{H}^+$	$7.5 \times 10^4 \text{ s}^{-1}$		4
B10	$\text{HO}_2^{\bullet} + \text{HO}_2^{\bullet} \rightleftharpoons \text{H}_2\text{O}_2 + \text{O}_2$	$8.3 \times 10^5 \text{ M}^{-1} \text{ s}^{-1}$		4
B11	$\text{HO}_2^{\bullet} + \text{O}_2^{\bullet-} \rightleftharpoons \text{HO}_2^- + \text{O}_2$	$9.7 \times 10^7 \text{ M}^{-1} \text{ s}^{-1}$		4
B12	$\text{H}_2\text{O}_2 \rightleftharpoons \text{HO}_2^- + \text{H}^+$	$1.2 \times 10^{-2} \text{ s}^{-1}$	From pK _a 11.62	7
B13	$\text{HO}_2^- + \text{H}^+ \rightleftharpoons \text{H}_2\text{O}_2$	$5 \times 10^9 \text{ M}^{-1} \text{ s}^{-1}$		

Text S4. Kinetic model used to fit the measured kinetic traces of $^3\text{DMABN}^*$, DMABN^{*+} and e_{aq}^- in degassed solution

Reaction equations (with corresponding rate constants given on the right):



Differential equations for the concentrations of $^3\text{DMABN}^*$ (c_{T}), e_{aq}^- (c_{e^-}), DMABN^{*+} (c_{RAD}) and DMABN^{*-} (c_{ANION}):

$$\frac{dc_{\text{T}}}{dt} = -k_0 \times c_{\text{T}} - (2 - \phi_{\text{isc}}) \times k_{\text{TT}} \times c_{\text{T}}^2 \quad (\text{S1})$$

$$\frac{dc_{e^-}}{dt} = -k_{e^-} \times c_{e^-} \times c_{\text{DMABN}} \quad (\text{S2})$$

$$\frac{dc_{\text{RAD}}}{dt} = -k_{\text{RAD}} \times c_{\text{RAD}} - k_{\text{redox}} \times c_{\text{RAD}} \times c_{\text{ANION}} \quad (\text{S3})$$

$$\frac{dc_{\text{ANION}}}{dt} = k_{e^-} \times c_{e^-} \times c_{\text{DMABN}} - k_{\text{redox}} \times c_{\text{RAD}} \times c_{\text{ANION}} \quad (\text{S4})$$

To describe the fate of the various transient species formed upon LFP of DMABN in degassed solution, we constructed a kinetic model based on processes A to G. Thereby, it is important to note that the excited singlet state of DMABN ($^1\text{DMABN}^*$) decays much faster than all other transient species. Equation S1 represents the differential rate equation for the deactivation of the excited triplet state of DMABN ($^3\text{DMABN}^*$, concentration defined as c_{T}), consisting of a unimolecular decay (Process A, with rate constant k_0) and a triplet–triplet annihilation process (Process B, with rate constant k_{TT}). The coefficient of the second-order member, i.e. $(2 - \phi_{\text{isc}})$, takes the reformation of $^3\text{DMABN}^*$ through intersystem crossing from $^1\text{DMABN}^*$ (which is a product of triplet–triplet annihilation) into account, whereby $\phi_{\text{isc}} = k_{\text{isc}} / (k_{\text{f}} + k_{\text{ic}} + k_{\text{isc}})$ is the intersystem crossing quantum yield (from $^1\text{DMABN}^*$). ϕ_{isc} is not known for aqueous solutions at room temperature, but was determined to be 0.80 and 0.55 in *n*-hexane and ethanol solutions, respectively.¹² For the present fitting procedure, the second value (i.e., 0.55) was employed. The

differential rate laws for the hydrated electron (e_{aq}^-) (Process C, with rate constant k_{e^-}), the radical cation of DMABN ($\text{DMABN}^{*\cdot+}$) (Processes D and G, with rate constants k_{redox} and k_{RAD} , respectively) and the radical anion of DMABN ($\text{DMABN}^{*\cdot-}$) (Processes C and D, with rate constants k_{e^-} and k_{redox} , respectively) are given in Equations S2–S4. $\text{DMABN}^{*\cdot-}$ does not absorb in the studied wavelength range, therefore only computed concentrations of this species, and not experimental absorption related to it, were used in the fitting procedure. The concentration of DMABN in the ground state was considered to be constant ($c_{\text{DMABN}} = 9 \times 10^{-5} \text{ M}$) during the reaction time, as we considered that c_{DMABN} was not significantly changing after excitation. The concentrations of $^3\text{DMABN}^*$ and $\text{DMABN}^{*\cdot+}$ obtained from minimization were about two orders of magnitude smaller ($c_{\text{T}} = 1.46 \times 10^{-6} \text{ M}$; $c_{\text{RAD}} = 8.8 \times 10^{-7} \text{ M}$) than c_{DMABN} . Therefore, we approximated the quenching of solvated electrons by ground-state DMABN (C, k_{e^-}) as a pseudo first order process.

To determine the rate constants of the individual deactivation processes of the transients (k_0 , k_{TT} , k_{e^-} , k_{redox} and k_{RAD}), absorbance kinetic traces of laser flash-excited DMABN ($c = 9 \times 10^{-5} \text{ M}$) in degassed aqueous solutions were measured at 400, 500 and 600 nm, where the absorption of three transients, $^3\text{DMABN}^*$, e_{aq}^- , and $\text{DMABN}^{*\cdot+}$ contributed to the kinetic traces. Note that the ground state of DMABN does not absorb at wavelengths longer than 360 nm.

The most accurate estimates of the rate constants were obtained by the global fit of the differential rate equations (Equations S1–S4) to three kinetic traces at 400, 500 and 600 nm measured under otherwise identical experimental conditions (see an example in Figure S9). For the fit of each kinetic trace, the initial concentrations of $^3\text{DMABN}^*$, e_{aq}^- and $\text{DMABN}^{*\cdot+}$ were set as initial estimates: The concentration of $^3\text{DMABN}^*$ was calculated from the absorbance at 400 nm, the concentration of $\text{DMABN}^{*\cdot+}$ was estimated from the absorbance at 500 nm and the concentration of e_{aq}^- was set equal to the concentration of $\text{DMABN}^{*\cdot+}$. The initial concentration of $\text{DMABN}^{*\cdot-}$ was set to zero as $\text{DMABN}^{*\cdot-}$ is formed only later through process C. The corresponding molar absorption coefficients of transients were taken from literature (see Table S4). The first-order (k_0 ; k_{RAD}); pseudo-first-order (k_{e^-}) and second-order (k_{TT}) rate constants obtained from the minimization of three sets of kinetic traces are summarized in Table S5.

Table S4. Molar absorption coefficients applied for the estimates of the initial concentrations of the transient species for the global fit

	Molar absorption coefficient / M ⁻¹ cm ⁻¹			Initial concentration / M
	at 400nm	at 500nm	at 600nm	
e_{aq}^- ^a	500	7600	12500	9.13×10^{-7}
³ DMABN* (in EtOH) ^b	8600	2600	4000	1.46×10^{-6}
DMABN ^{•+} ^c	-	2100	-	9.13×10^{-7}

Notes: ^afrom Ref. 6 , ^bfrom Ref. 12, ^c estimated using the absorbance data from a DMABN photoionization experiments assuming equimolar production of e_{aq}^- and of DMABN^{•+} and calculating the concentration of e_{aq}^- produced using its literature molar absorption coefficient.

Table S5. Rate constants of the studied transients obtained from three independent measurements by applying the global fitting procedure described above

k_0 / s^{-1}	$k_{\text{TT}} / \text{M}^{-1} \text{s}^{-1}$	$k_{\text{e}^-} / \text{M}^{-1} \text{s}^{-1}$	$k_{\text{redox}} / \text{M}^{-1} \text{s}^{-1}$	$k_{\text{RAD}} / \text{s}^{-1}$
$(3.92 \pm 0.12) \times 10^4$	$(5.86 \pm 0.21) \times 10^8$	$(1.05 \pm 0.07) \times 10^{10}$	$(5.0 \pm 0.8) \times 10^8$	$(4.8 \pm 1.2) \times 10^3$

Note: Values are given as (average \pm standard deviation).

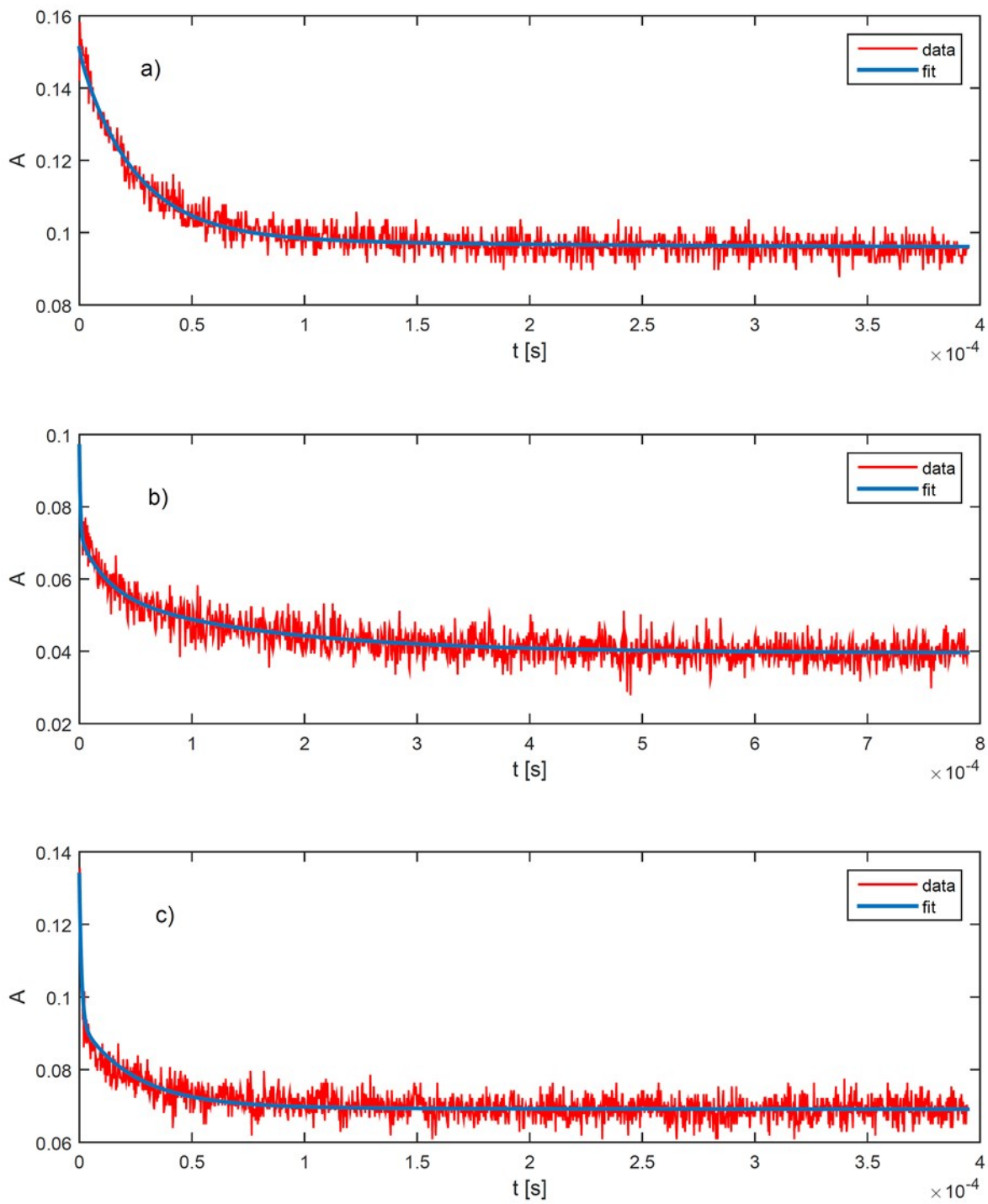


Figure S1. Fits of the kinetic traces measured at: (a) 400 nm, (b) 500 nm and (c) 600 nm.

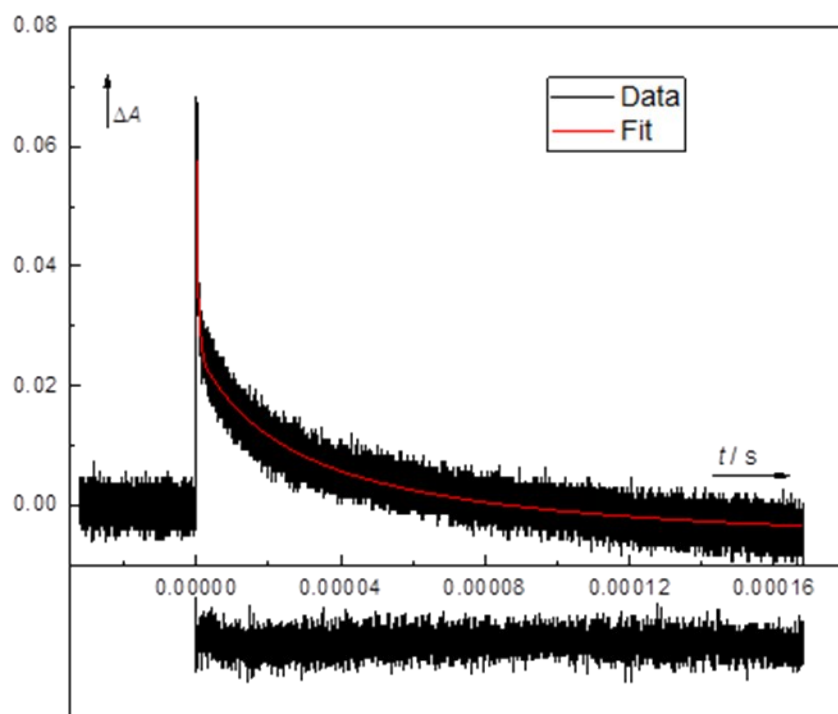


Figure S2. Kinetic trace recorded upon DMABN excitation ($[\text{DMABN}] = 1.33 \times 10^{-4} \text{ M}$, laser pulse energy: 70 mJ, excitation wavelength: 266 nm) in aerated aqueous solution, measured at $\lambda = 500 \text{ nm}$ and fitted using a second-order rate constant for the decay of $\text{DMABN}^{\bullet+}$ and two fixed first-order rate constants for the decay of the hydrated electron and $^3\text{DMABN}^*$.

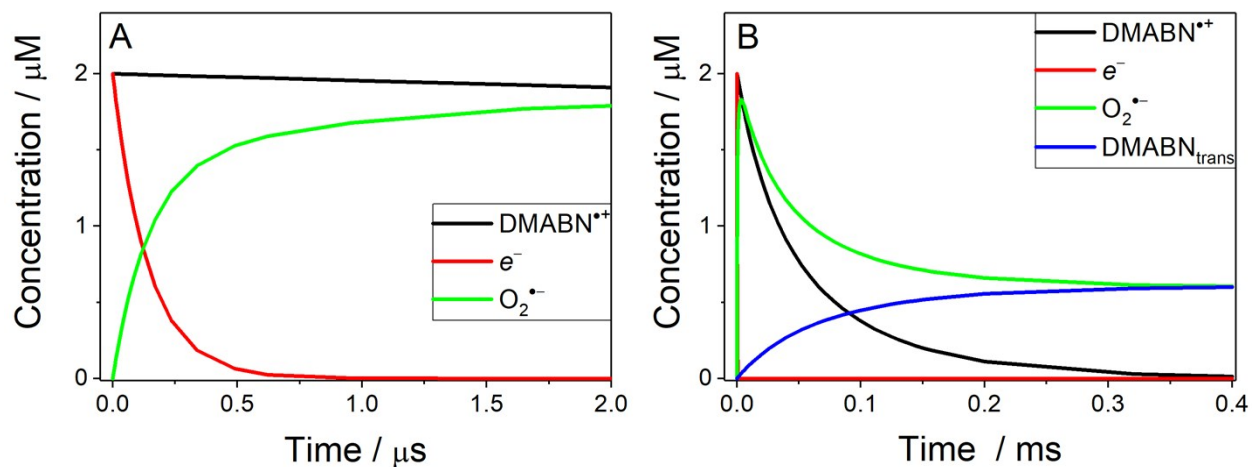


Figure S3. Kinetic simulations showing the evolution of the concentration of selected species of interest (DMABN^{*+}, e_{aq}⁻, O₂^{•-} and DMABN_{trans}) formed upon 266 nm laser pulse excitation of an aerated solution of DMABN (A) on a microsecond time scale and (B) on a millisecond time scale. Starting reactant concentrations: [DMABN^{*+}] = [e_{aq}⁻] = 2×10^{-6} M, [O₂] = 2.8×10^{-4} M, [DMABN_{trans}] = 0 M; pH 7.7. Starting concentrations of the transients were set to approximately match the maximum experimental concentration of DMABN^{*+} determined at a delay time of 2 μs after the laser pulse.

Table S6. Kinetic parameters determined for the deactivation of ³DMABN* and DMABN⁺⁺ formed during 266 nm laser flash photolysis of aqueous DMABN in aerated and N₂O-purged solutions at various pH values. ^a

Transient species	Air			N ₂ O		
	³ DMABN*		DMABN ⁺⁺	³ DMABN*		DMABN ⁺⁺
pH	$k_{3DMABN^*}^{d,obs} / 10^6$ s ⁻¹	$k_{3DMABN^*,O_2}^{q,exp} / 10^9$ M ⁻¹ s ⁻¹	$k_{DMABN^{++},O_2}^{q,exp} / 10^9$ M ⁻¹ s ⁻¹	$k_{3DMABN^*}^{d,obs} / 10^5$ s ⁻¹	$k_{3DMABN^*,N_2O}^{q,exp} / 10^7$ M ⁻¹ s ⁻¹	$k_{DMABN^{++}}^{d,obs} / 10^4$ s ⁻¹
4.5	1.82 ± 0.01	6.36	4.0 ± 0.2	2.79 ± 0.02	0.89	0.9 ± 0.1
5.4	1.76 ± 0.02	6.14	7.71 ± 0.07	3.67 ± 0.08	1.21	0.96 ± 0.06
6.2	1.77 ± 0.01	6.18	8.0 ± 0.2	4.02 ± 0.08	1.34	1.09 ± 0.14
7	1.71 ± 0.01	5.96	7.1 ± 0.3	3.89 ± 0.03	1.29	1.25 ± 0.12
7.7	1.70 ± 0.02	5.93	8.1 ± 0.5	6.47 ± 0.02	2.4	1.24 ± 0.07

Note: ^a See Table 1 in the main paper for definitions and conditions.

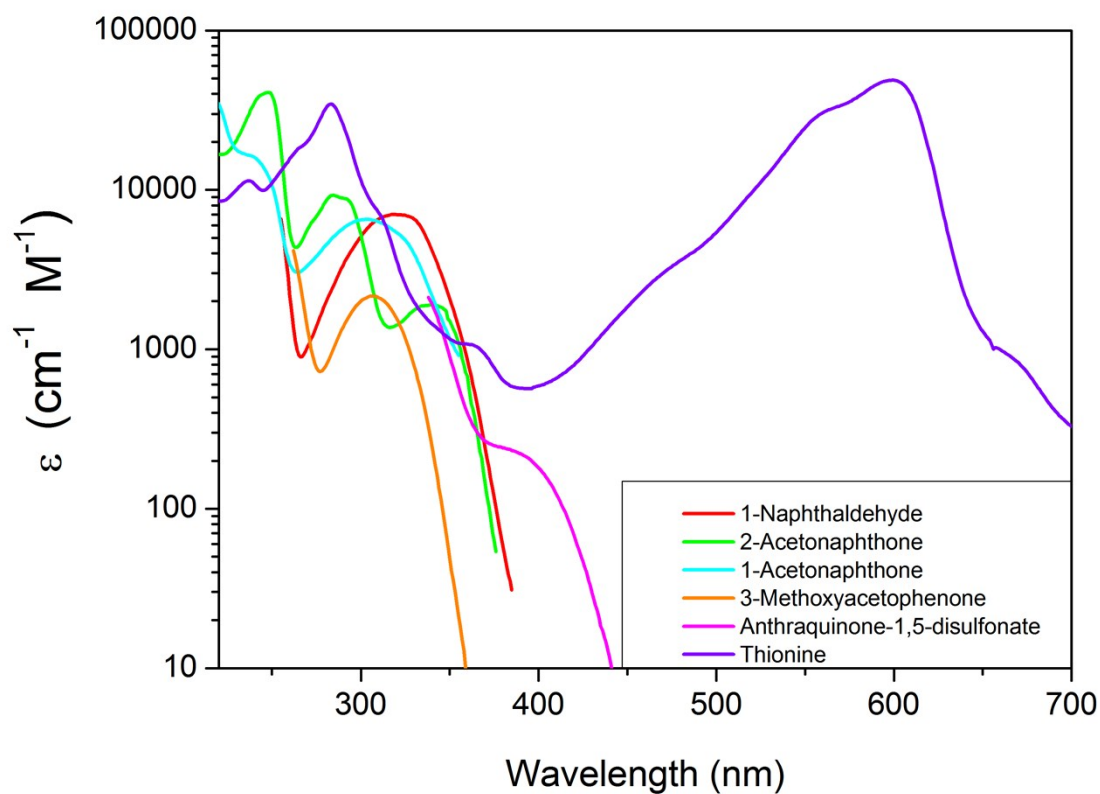


Figure S4. Absorption spectra of the photosensitizers used during the experiments, measured in pH 8 phosphate-buffered aqueous solution (containing small amounts of acetonitrile as a co-solvent in the case of 1-naphthaldehyde (0.6% v/v) and 3-methoxy-acetophenone (10% v/v)).

Text S5. Transient absorption spectra of species observed in the 1-naphthaldehyde (1-NA) system

The absorption spectrum of the triplet state of 1-NA ($^31\text{-NA}^*$) has a broad maximum centered at ≈ 500 nm (Figure S5A).^{8,9} A band centered at ≈ 420 nm can be attributed to the radical anion of 1-NA (Figure S5B). The DMABN $^{+}$ band can be observed at ≈ 500 nm on a long timescale in the 1-NA + DMABN system (Figure S5C).

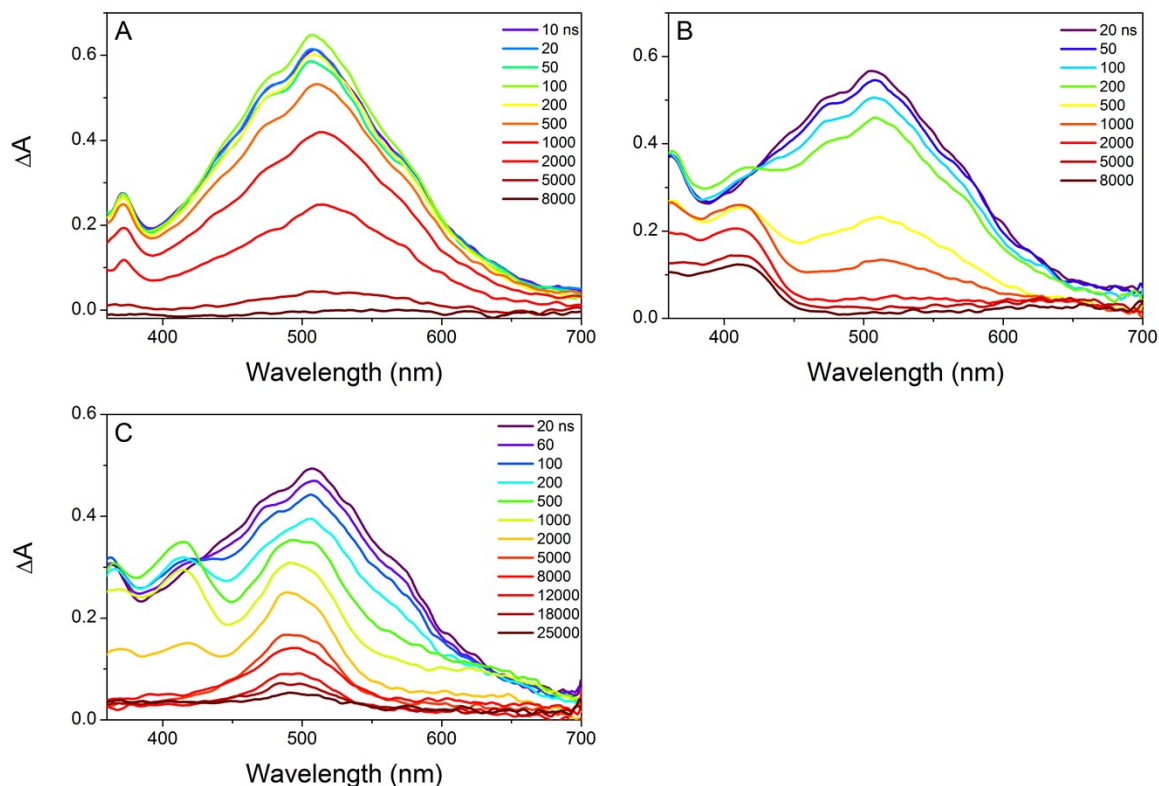


Figure S5. Transient absorption spectra measured after a 355nm laser pulse in pH 8 aerated conditions of solutions containing: (A) 1-Naphthaldehyde (1-NA, 3.0×10^{-4} M). (B) 1-NA (3.0×10^{-4} M) + triethanolamine (TEA, 1.0×10^{-2} M). (C) 1-NA (3.0×10^{-4} M) + DMABN (5.0×10^{-4} M). Data were smoothed by adjacent averaging over 20 data points (≈ 10 nm).

Text S6. Transient absorption spectra of species observed in the 1-acetonaphthone (1-AN) system

The absorption spectrum of the triplet state of 1-AN ($^3\text{1-AN}^*$) has a maximum centered at $\lambda \approx 500$ nm (Figure S6A). No additional species were observable in the 1-AN + DMABN system (Figure S6B), probably because of the low reactivity of DMABN towards $^3\text{1-AN}^*$.

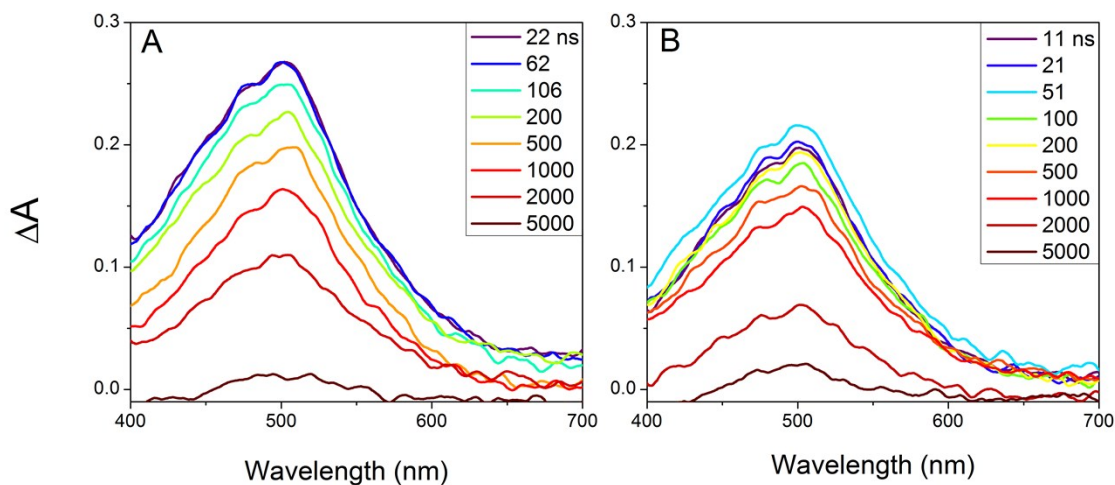


Figure S6. Transient absorption spectra measured after a 355 nm laser pulse in pH 8 aerated conditions of solutions containing: (A) 1-Acetonaphthone (1-AN, 2.5×10^{-4} M). (B) 1-AN (2.5×10^{-4} M) + DMABN (5.0×10^{-4} M). Data were smoothed by adjacent averaging over 20 data points (≈ 10 nm).

Text S7. Transient absorption spectra of species observed in the 9,10-anthraquinone-1,5-disulfonate (AQdS) system

The absorption spectrum of the triplet state of AQdS ($^3\text{AQdS}^*$) exhibits a maximum at ≈ 400 nm (Figure S7A). The radical anion of AQdS ($\text{AQdS}^{\bullet-}$) was produced by electron transfer from nitrite to $^3\text{AQdS}^*$ and shows an absorption band centered at ≈ 520 nm (Figure S7B).¹⁰

The absorption spectrum of $\text{DMABN}^{\bullet+}$ overlaps with the one of $\text{AQdS}^{\bullet-}$ (Figure S7C), making the AQdS system unpractical for the measurement of $\text{DMABN}^{\bullet+}$.

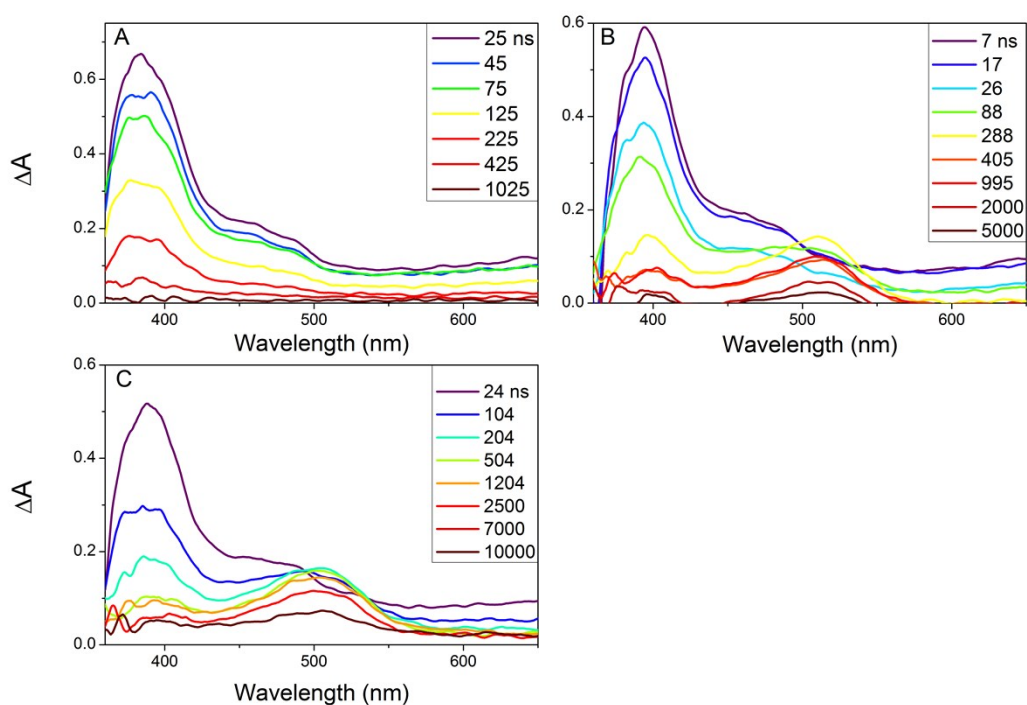


Figure S7. Transient absorption spectra measured after a 355 nm laser pulse in pH 8 aerated aqueous solutions containing: (A) 9,10-Anthraquinone-1,5-disulfonate (AQdS, 1.0×10^{-3} M). (B) AQdS (1.0×10^{-3} M) + NaNO_2 (1.0×10^{-2} M). (C) AQdS (1.0×10^{-3} M) + DMABN (4.0×10^{-4} M). Data were smoothed by adjacent averaging over 20 data points (≈ 10 nm).

Text S8. Transient absorption spectra of species observed in the thionine (THI) system

Upon LFP of a thionine (THI) solution, the triplet state absorption spectrum of THI as well as the ground state bleaching of THI, giving rise to a negative differential absorbance, can be observed (Figure S8A). This complexity in transient spectra is due to the fact that THI significantly absorbs light across the whole observation spectral window (Figure S1), which was not the case for the other photosensitizers. In the presence of triethanolamine (TEA), the radical anion of THI can be observed with an absorption band at ≈ 400 nm (Figure S8B). DMABN^{•+} can be observed on a long timescale in the THI + DMABN system (Figure S8C).

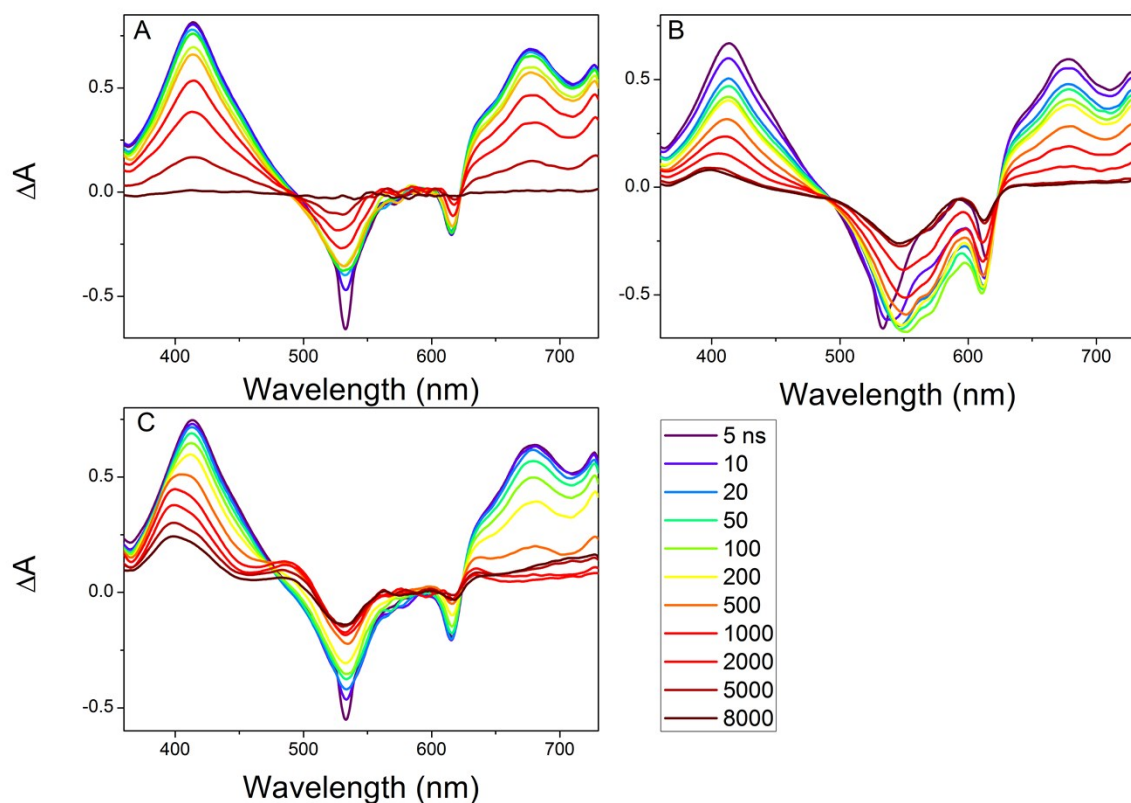


Figure S8. Transient absorption spectra measured after a 532 nm laser pulse in pH 8 aerated conditions of solutions containing: (A) Thionine (THI, 3.5×10^{-5} M). (B) THI (3.5×10^{-5} M) + TEA (1.0×10^{-2} M). (C) THI (3.5×10^{-5} M) + DMABN (5.0×10^{-4} M). Data were smoothed by adjacent averaging over 20 data points (≈ 10 nm).

Text S9. Transient absorption spectra of species observed in the 3-methoxyacetophenone (3-MOAP) system

The absorption spectrum of the triplet state of 3-MOAP ($^33\text{-MOAP}^*$) exhibits a maximum at ≈ 400 nm and a shoulder at ≈ 440 nm (Figure S9A).¹¹ The spectrum of the radical anion of 3-MOAP overlaps with the one of the triplet state with an absorption centered at 420 nm. (Figure S9B).

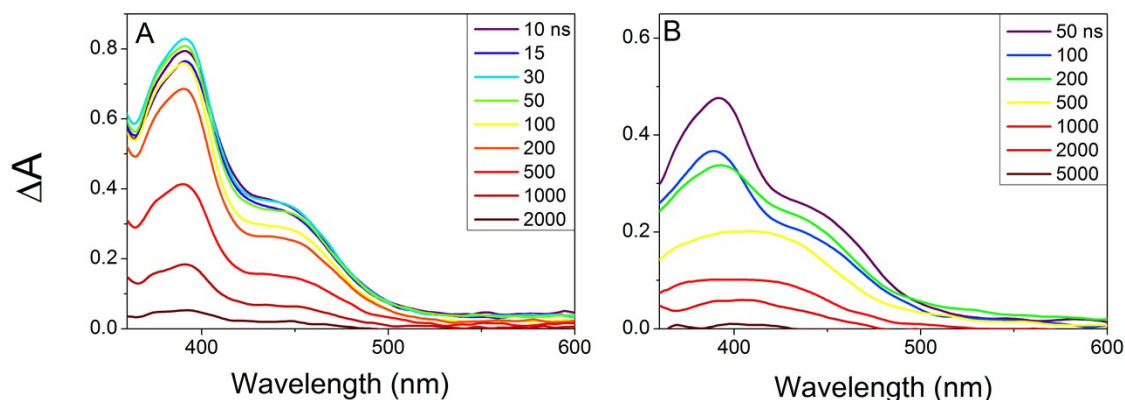


Figure S9. Transient absorption spectra measured after a 355 nm laser pulse in pH 8 aerated conditions of solutions containing: (A) 3-Methoxyacetophenone (3-MOAP, 1.0×10^{-2} M). (B) 3-MOAP (1.0×10^{-2} M) + TEA (1.0×10^{-2} M). The solutions contain 10% (v/v) acetonitrile as co-solvent. Data were smoothed by adjacent averaging over 20 data points (≈ 10 nm).

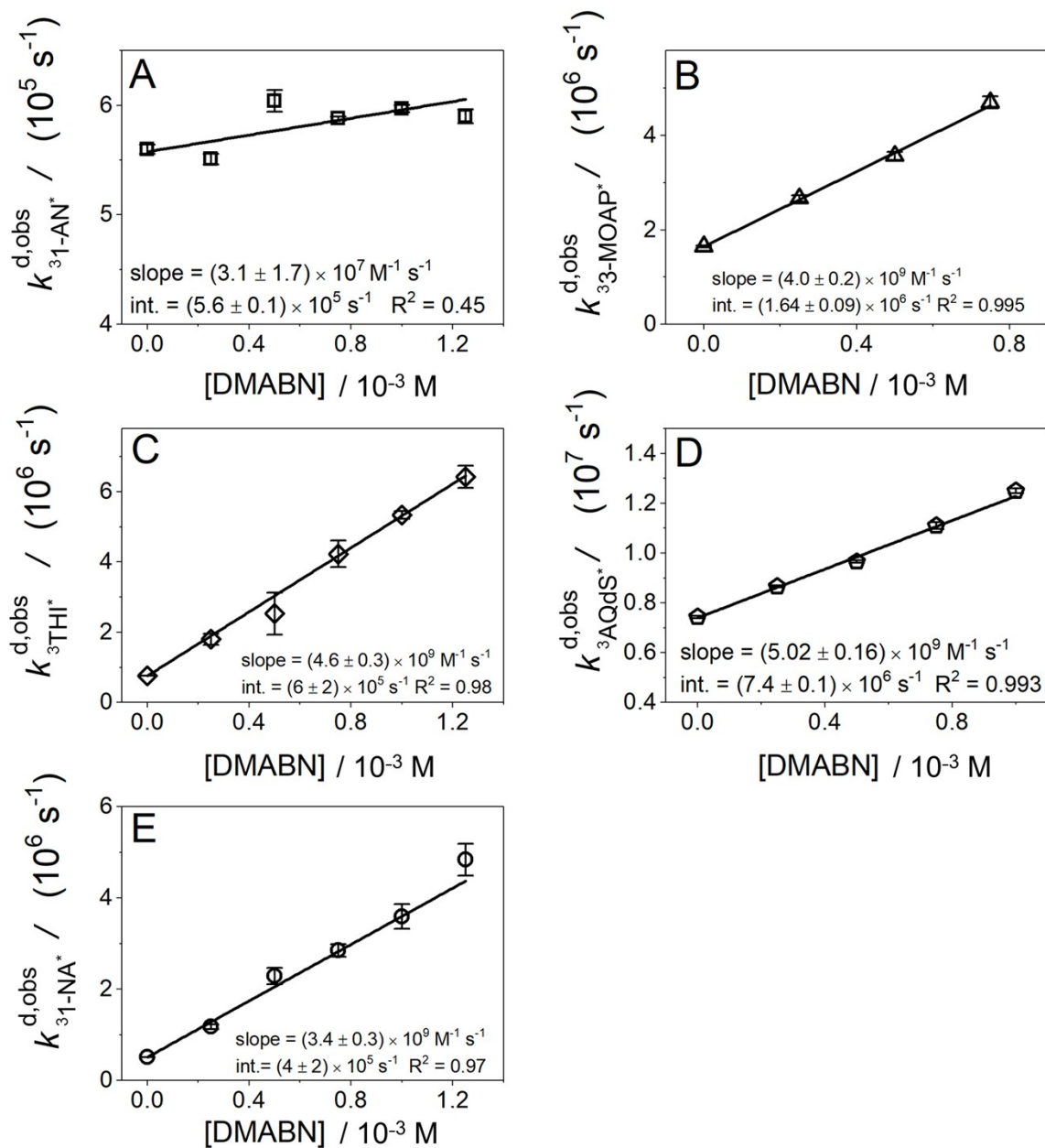


Figure S10. Plots with linear regressions used for the determination of the second-order rate constant of the quenching of excited triplet states of photosensitizers by DMABN (see Table 2 in the main paper). (A) 1-Acetonaphthone ($1.0 \times 10^{-3} M$); (B) 3-Methoxyacetophenone ($1.0 \times 10^{-2} M$, with 10% (v/v) acetonitrile as a co-solvent); (C) Thionine ($5.0 \times 10^{-5} M$); (D) 9,10-Anthraquinone-1,5-disulfonate ($1.0 \times 10^{-3} M$). (E) 1-Naphthaldehyde ($3.0 \times 10^{-4} M$, with 0.6% (v/v) acetonitrile as a co-solvent). All measurements were done in aerated pH 8 phosphate-buffered solutions.

Text S10. Conventional second-order kinetic analysis of the decay of DMABN^{•+} formed by photosensitization using 1-naphthaldehyde (1-NA)

The transient absorbance change data, ΔA_{500} (where ΔA_{500} was measured at the wavelength of 500 nm over the 4.0 cm path length of the employed quartz cuvette), were analyzed using conventional second-order kinetic plots of $1/\Delta A_{500}$ vs. time in the time range of 6 – 84 μ s delay after the laser pulse. These plots yielded straight lines with high determination coefficients (see Figure S11 and Table S7 below). The obtained slopes of the linear regression lines were stable for the three higher initial ³1-NA* concentrations (on average $(1.926 \pm 0.003) \times 10^6 \text{ s}^{-1}$) but increased with decreasing concentration of ³1-NA* as obtained by using the metal grid filters, reaching a ≈ 2 times higher value than the abovementioned one at the lowest examined concentration. This is interpreted, despite the excellent correlation coefficients, as a deviation from second-order kinetics with increasing mixing of a first-order component with decreasing initial [³1-NA*]. When fitting the data over a longer time range (up to 160 μ s, data not shown), determination coefficients decreased with decreasing initial [³1-NA*], confirming the postulated deviation from second-order kinetics. From the above average slope, an average second-order rate constant of $(1.618 \pm 0.003) \times 10^{10} \text{ M}^{-1} \text{ s}^{-1}$ was obtained by applying a molar absorption coefficient of $\approx 2100 \text{ M}^{-1} \text{ cm}^{-1}$ for DMABN^{•+}.

We assign this rate constant to $k_{DMABN^{\cdot+}, O_2^{\cdot-}}^{q,exp}$, the second-order rate constant for the reaction of DMABN^{•+} with O₂^{•-} (Equation 13 in the main paper).

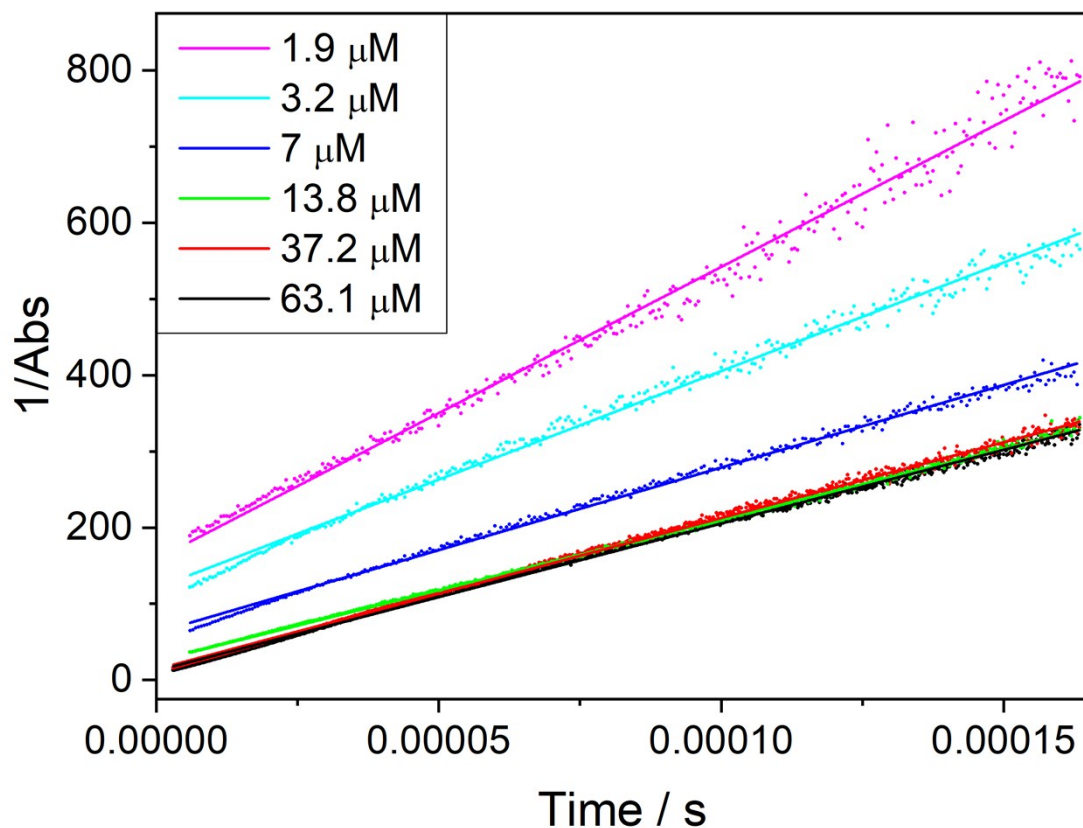


Figure S11. Second-order kinetics plots and linear regression lines for the transient absorbance change data corresponding to the decay of DMABN^{•+} formed by photosensitization using 1-NA. The estimated initial concentration of the triplet state of 1-NA is given in the legend and was calculated according to the details specified in Table S7. Further experimental conditions and obtained regression parameters values are also given in Table S7.

Table S7. Parameter values and rate constants obtained from the conventional second-order kinetic analysis (see linear regressions shown in Figure S11).

[1-NA] / 10 ⁻⁶ M	[³ 1-NA*] ₀ ^a / 10 ⁻⁶ M	Slope / s ⁻¹	Intercept	R ²	$k_{\text{DMABN}^{\cdot+}, \text{O}_2^{\cdot-}}^{\text{q,exp}}$ / M ⁻¹ s ⁻¹
300	63.1	(1.933 ± 0.003) × 10 ⁶	12.1 ± 0.3	0.998	(1.623 ± 0.003) × 10 ¹⁰
150	37.2	(1.987 ± 0.003) × 10 ⁶	13.9 ± 0.3	0.998	(1.669 ± 0.003) × 10 ¹⁰
50	13.8	(1.858 ± 0.004) × 10 ⁶	24.9 ± 0.4	0.999	(1.561 ± 0.003) × 10 ¹⁰
50^b	7.0	(2.167 ± 0.007) × 10 ⁶	62.1 ± 0.7	0.997	(1.820 ± 0.006) × 10 ¹⁰
50^c	3.2	(2.848 ± 0.013) × 10 ⁶	120.6 ± 1.3	0.993	(2.393 ± 0.011) × 10 ¹⁰
50^d	1.9	(3.84 ± 0.02) × 10 ⁶	158 ± 2	0.988	(3.22 ± 0.02) × 10 ¹⁰

Notes: ^a The estimation of the starting concentration of the triplet of 1-NA, [³1-NA*]₀, was done assuming an average energy of 150 mJ per laser pulse distributed equivalently over the 4×1cm side of the quartz cuvette, the reduction of the light intensity by the metal filters, the absorption of light by the solution calculated using a molar absorption coefficient at 355 nm of 1372 M⁻¹ cm⁻¹ for 1-NA and a unity intersystem crossing quantum yield to form ³1-NA*. ^b in the presence of a 46% transmittance metal filter. ^c in the presence of a 20% transmittance metal filter. ^d in the presence of a 12% transmittance metal filter.

Table S8. Parameters values obtained by the Kintecus[®] fits applied to the decay data of DMABN^{•+} formed by photosensitization using 1-NA. ^a

[1-NA] / 10⁻⁶ M	[³1-NA*]₀ ^b / 10⁻⁶ M	$k_{\text{DMABN}^{\bullet+}, \text{O}_2}^{\text{q,exp}}$ / M⁻¹ s⁻¹	$\epsilon_{\text{DMABN}^{\bullet+}}$ / M⁻¹ cm⁻¹	$k_{\text{DMABN}^{\bullet+}}^{\text{d,obs}}$ ^c / s⁻¹
300	63.1	$(4.5 \pm 0.4) \times 10^9$	2338 ± 169	100
150	37.2	$(5.8 \pm 0.3) \times 10^9$	2847 ± 112	100
50	13.8	$(6.4 \pm 0.1) \times 10^9$	3464 ± 83	100
50^d	7	$(8.53 \pm 0.02) \times 10^9$	3474 ± 0	100
50^e	3.2	$(1.11 \pm 0.07) \times 10^{10}$	3691 ± 167	100
50^f	1.9	$(1.23 \pm 0.04) \times 10^{10}$	3856 ± 207	$(1.2 \pm 0.5) \times 10^3$

Notes: ^a obtained values expressed as mean \pm s.d. ^b The estimation of the starting concentration of the triplet of 1-NA, [³1-NA*]₀, was done as described in Table S7. ^c the value was constrained to a minimum of 100 s⁻¹. ^d in the presence of a 46% transmittance metal filter. ^e in the presence of a 20% transmittance metal filter. ^f in the presence of a 12% transmittance metal filter.

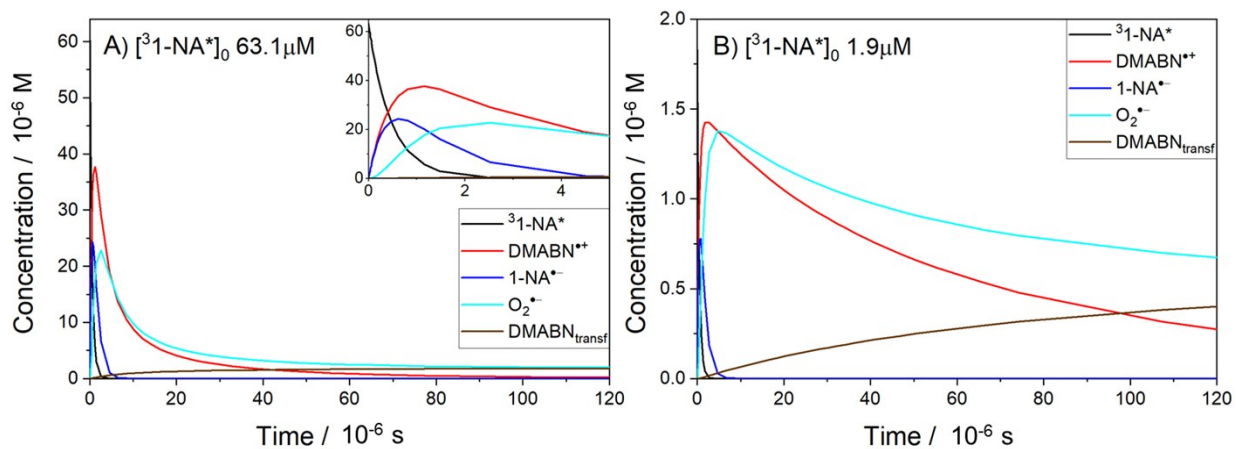


Figure S12. Kintecus[®] simulations using the system described in Text S3 and Table S3 for the reactions occurring in solutions containing 5×10^{-4} M DMABN and assuming initial concentrations of ${}^3\text{1-NA}^*$ of (A) 63.1 μM , and (B) 1.9 μM , corresponding to the minimum and maximum values of $[{}^3\text{1-NA}^*]_0$, respectively, according to Table S7. The insert in panel A represent the initial part of the same decay data at an expanded time scale.

References

1. J. C. Ianni, Kintecus Windows version 5.20, 2014. www.kintecus.com (accessed August 2016).
2. M. Anbar and E. J. Hart, Reactivity of aromatic compounds toward hydrated electrons, *J. Am. Chem. Soc.*, 1964, **86**, 5633-5637.
3. F. Leresche, U. von Gunten and S. Canonica, Probing the photosensitizing and inhibitory effects of dissolved organic matter by using *N,N*-dimethyl-4-cyanoaniline (DMABN), *Environ. Sci. Technol.*, 2016, **50**, 10997-11007.
4. B. H. J. Bielski, D. E. Cabelli, R. L. Arudi and A. B. Ross, Reactivity of HO₂/O₂⁻ radicals in aqueous solution, *J. Phys. Chem. Ref. Data*, 1985, **14**, 1041-1100.
5. E. Janata and R. H. Schuler, Rate constant for scavenging e_{aq}⁻ in N₂O-saturated solutions, *J. Phys. Chem.*, 1982, **86**, 2078-2084.
6. G. V. Buxton, C. L. Greenstock, W. P. Helman and A. B. Ross, Critical review of rate constants for reactions of hydrated electrons, hydrogen atoms and hydroxyl radicals (•OH/•O⁻) in aqueous solution, *J. Phys. Chem. Ref. Data*, 1988, **17**, 513-886.
7. W. M. Haynes, *CRC handbook of chemistry and physics*, CRC press, 2014.
8. A. Treinin and E. Hayon, Quenching of triplet states by inorganic ions. Energy transfer and charge transfer mechanisms, *J. Am. Chem. Soc.*, 1976, **98**, 3884-3891.
9. A. Samanta and R. W. Fessenden, On the triplet lifetime and triplet-triplet absorption spectra of naphthaldehydes, *Chem. Phys. Lett.*, 1988, **153**, 406-410.
10. J. N. Moore, D. Phillips, N. Nakashima and K. Yoshihara, Photophysics and photochemistry of sulfonated derivatives of 9,10-anthraquinone - Strong versus weak sensitizers, *J. Chem. Soc., Faraday Trans. 2*, 1987, **83**, 1487-1508.
11. H. Shizuka and H. Obuchi, Anion-induced triplet quenching of aromatic ketones by nanosecond laser photolysis, *J. Phys. Chem.*, 1982, **86**, 1297-1302.
12. G. Köhler, G. Grabner and K. Rotkiewicz, Nonradiative deactivation and triplet states in donor aryl acceptor compounds (dialkylaminobenzonitriles), *Chem. Phys.*, 1993, **173**, 275-290.